Applied Physics A (2020) 126:657
https://doi.org/10.1007/s00339-020-03857-z

Applied Physics A
Materials Science & Processing

Restoring and enhancing the coercivity of waste sintered (Nd,Ce,Gd)FeB magnets by direct Pr–Tb–Cu grain boundary diffusion

Yukun Liu[1] · Jiayi He[1] · Hongya Yu[1] · Zhongwu Liu[1] · Guoqing Zhang[2]

Received: 15 May 2020 / Accepted: 26 July 2020 / Published online: 2 August 2020

Abstract
A large amount of wastes are generated during sintered NdFeB production, and recycling of those wastes shows huge economic and environmental benefits. In this work, grain boundary diffusion process is employed to enhance the coercivity of waste sintered (Nd,Ce,Gd)FeB magnets. $Pr_{40}Tb_{30}Cu_{30}$ alloy is employed as the diffusion source. The coercivity of the waste magnet increased from 763 to 1287 kA/m without a consumption of remanence by optimized diffusion treatment. The maximum energy product and temperature stability of the magnets were also improved. The waste N30 magnet was successfully upgraded to N30M, close to N30H. It is found that that the shell/core structure with a Tb/Pr-rich shell and Nd/Ce/Gd-rich core was formed in the grain boundary diffused magnets, which is the main reason for the enhancement of coercivity and temperature stability. The detailed investigations clarified the distribution preference of different rare earth elements. Tb prefers entering into the main phase, while Pr tends to diffuse along the grain boundaries with large diffusion depth. The Nd, Ce and Gd elements also show different capacities of being replaced. These results suggest that the grain boundary diffusion process can be used as an efficient recycling method for those waste NdFeB magnets which were not seriously oxidized.

Keywords Nd–Fe–B magnets · Waste sintered magnets · Grain boundary diffusion · Coercivity · Microstructure

1 Introduction

With the expansion of application fields, NdFeB magnets play an increasingly important role in modern industry [1, 2]. In recent years, the output of NdFeB showed a significant growth, which is also expected in the next couple of years [3]. Presently, over 90% of NdFeB magnets are fabricated by the sintering process. However, during the traditional processing of sintering, a large amount of raw materials are converted into NdFeB wastes. If the magnets after their life cycles are included, the total amount of NdFeB wastes is huge. Developing environmentally friendly and cost-effective recycling processes is very crucial for the NdFeB industry and related fields [4].

✉ Zhongwu Liu
zwliu@scut.edu.cn

[1] School of Material Science and Engineering, South China University of Technology, Guangzhou 510640, China

[2] Advanced High Temperature Structural Materials Laboratory, Beijing Institute of Aeronautical Materials, Beijing 100095, China

There are two types of NdFeB wastes, including seriously oxidized wastes and non-oxidized wastes. For the former, direct use of the waste magnets is difficult. A common method is to extract the valuable elements, especially the rare earth elements (REEs), from the wastes [5–8]. For example, REEs can be recovered from NdFeB magnet wastes by selective chlorination using NH_4Cl [9], $FeCl_2$ [10] or $MgCl_2$ [6]. For the latter, the extraction process seems costly and unnecessary. Directly preparing the NdFeB-type materials or other magnetic materials, such as regenerated magnetic powders [11–13], regenerated sintered magnets [11, 14], regenerated bonded magnets [15, 16] and wave absorbing materials [17], for certain applications from the NdFeB wastes has become achievable. Regenerating NdFeB magnets from wastes has already been employed in industry and proved effective; however, the pulverization or remelting process is still essential, and the reproduced magnets show inferior magnetic properties to those made from fresh powders. Hence, industries are eagerly looking for simple and effective recycling processes.

Since formally proposed in 2005 [18], grain boundary diffusion process (GBDP) has been widely accepted as an effective method to enhance the coercivity of NdFeB

magnets in both laboratory and industry [19–22]. The alloys or compounds containing heavy rare earth element (HREE) are used as the diffusion sources. The formation of shell/core structure is believed to be the key mechanism of coercivity enhancement in this Tb/Dy introduced GBDP. Since 2010, it has also been proved that the eutectic Pr/Nd-M (M: low melt point metal such as Cu and Al) alloys can also be used as diffusion sources, and they improve the coercivity by modifying the grain boundary. Industrially, GBDP has been employed to fabricate the commercial NdFeB magnets with extremely high coercivity, but it also provides us a new approach to enhance the performance of waste magnets. Our previous work [23] has shown that the coercivity of waste NdFeB magnets can be enhanced by Pr–Cu diffusion treatment.

On the other hand, light rare earth elements (LREs) such as Ce, La, Gd, and Y have been frequently employed to substitute Nd in NdFeB magnets for improving performance/cost ratio of the low grade magnets. Due to the low intrinsic magnetic properties of $RE_2Fe_{14}B$ phase (2:14:1 phase) formed by LREs [24], the decrease of magnetic properties is inevitable. How to enhance their properties, especially the coercivity, is also a major topic [25–27].

In this work, GBDP is employed for restoring and enhancing the coercivity of the waste (Nd,Ce,Gd)FeB magnets. Ternary Pr–Tb–Cu alloy was employed as the diffusion source, which is expected to combine the advantages of HRE and eutectic alloy diffusion sources. In addition, the relatively low melt point of this ternary alloy can contribute to the formation of RE rich with good wettability, leading to the high diffusion efficiency of Tb atoms. The magnetic properties and microstructures of the waste NdFeB magnets before and after GBDP were analyzed in this paper. The diffusion behavior of REEs were also investigated in detail.

2 Experimental

The waste sintered NdFeB magnets, containing relatively large amount of LREs of Ce and Gd, was taken from the production line of low-grade magnets N30, which are only slight oxidized. The wastes were cut into a size of $7\times7\times2$ mm as the diffusion substrate with the *c*-axis parallel to the 2 mm side. The $Pr_{40}Tb_{30}Cu_{30}$ ribbon was used as diffusion source, which was prepared by arc melting using 99.9% pure elements and melt-spun at a wheel with a speed of 30 m/s. The melting point of the $Pr_{40}Tb_{30}Cu_{30}$ alloy was determined as 600 °C by differential scanning calorimetry (not shown here). The 7×7 mm surfaces of the magnets were coated with the melt-spun ribbons. Two consecutive heat treatments under vacuum, i.e., 800–900 °C for 2–8 h followed by 460–540 °C for 3 h were employed for diffusion.

The magnetic properties at room temperature and from 300 to 450 K were measured by a vibrating sample magnetometer in the physical property measurement system (PPMS, Quantum Design, PPMS-9) with a maximum field of 5 T along the *c*-axis of the magnet. The microstructures were investigated by a scanning electron microscope (SEM, FEI NOVA NANOSEM 430) and electron probe microanalyzer (EPMA, Shimadzu, EPMA-1600). Transmission electron microscopy (TEM) observations were performed using FEI Tecnai G2 F20 S-TWIN with an acceleration voltage of 200 kV.

3 Results and discussion

The magnetic properties of the initial (Nd,Ce,Gd)FeB waste magnets (N30) were characterized in the beginning. The coercivity (H_{cj}), remanence (J_r) and maximum energy product ($(BH)_{max}$) were characterized to be 763 kA/m, 1.08 T and 202 kJ/m^3, respectively. Compared to the standard of N30 magnet, i.e., $H_{cj} \geq 960$ kA/m, $J_r \geq 1.08$ T, and $(BH)_{max} \geq 223$ kJ/m^3, the waste magnets have both lower coercivity and lower maximum energy product. Here, it should be noted that all standards for the properties of Nd–Fe–B magnets in this paper refer to the Chinese National Standard, GB/T 13560-2017. Figure 1 shows the SEM image of the initial magnets. A large amount of RE-rich phase aggregation was found in the magnet, and the areal fraction of the RE-rich phase was estimated to be 10.3% by calculation from Fig. 1 based on binarization, which is higher than that of ordinary NdFeB magnets. Except the main phase and RE-rich phase, some pores were also found in the magnets. These non-hard magnetic areas lead to a deterioration of magnetic performance, especially the J_r. The energy-dispersive spectroscopy (EDS) point analysis was

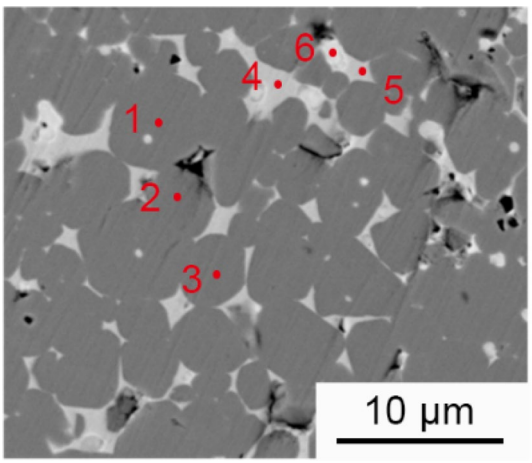

Fig. 1 SEM image of the waste-sintered NdFeB magnet

employed to observe the element distribution. The results are summarized in Table 1. Points 1, 2 and 3 are from the main phase of the 2:14:1 phase, and Points 4, 5 and 6 are from the RE-rich phases. The present magnets contain a large amount of Ce + Gd. Due to the relatively low intrinsic properties of $Ce_2Fe_{14}B$ and $Gd_2Fe_{14}B$, the magnetic properties of wastes are limited. Assuming the saturation magnetization of the $(Nd,Ce,Gd)_2Fe_{14}B$ phase is a linear superposition by the 2:14:1 phases of Nd, Ce and Gd, the saturation magnetization of the main phase can be estimated to be ~ 1.35 T, which is the main reason for insufficient J_r. In addition, some white areas such as Point 6 were noticed in Fig. 1. These parts were significantly oxidized grain boundary phase and consumed more Nd elements, having a negative effect on the magnetic performance. The analysis of initial magnets suggests that the low density and local oxidation, except the composition effect, may result in the low magnetic properties in the waste magnets.

The diffusion heat treatment was optimized, as demonstrated in Fig. 2. Two-stage heat treatment was carried out for all samples. Figure 2a, c show the magnetic properties of the magnets prepared with different first-stage heat treatments, i.e., 800–900 °C for 2–8 h, while the second-stage heat treatment was fixed at 500 °C/3 h. It is found that the H_{cj} and $(BH)_{max}$ increased with the increase of heat treatment temperature, which indicated that the short-term heat treatment was not sufficient for diffusion. The relatively high H_{cj} and $(BH)_{max}$ were obtained after diffusion

Table 1 Results of elemental point analysis in Fig. 1

Wt%	O	Al	Fe	Cu	Ce	Nd	Gd	Total
Point 1	0	0.62	75.76	0	7.89	10.30	5.42	100.00
Point 2	0	0.65	75.73	0	8.13	10.44	5.06	100.00
Point 3	0	0.58	75.84	0	8.14	10.16	5.28	100.00
Point 4	0	0	44.09	0.10	46.27	9.54	0	100.00
Point 5	0	0	45.51	0.06	47.88	6.55	0	100.00
Point 6	19.96	0	4.85	0.17	21.88	41.06	12.08	100.00

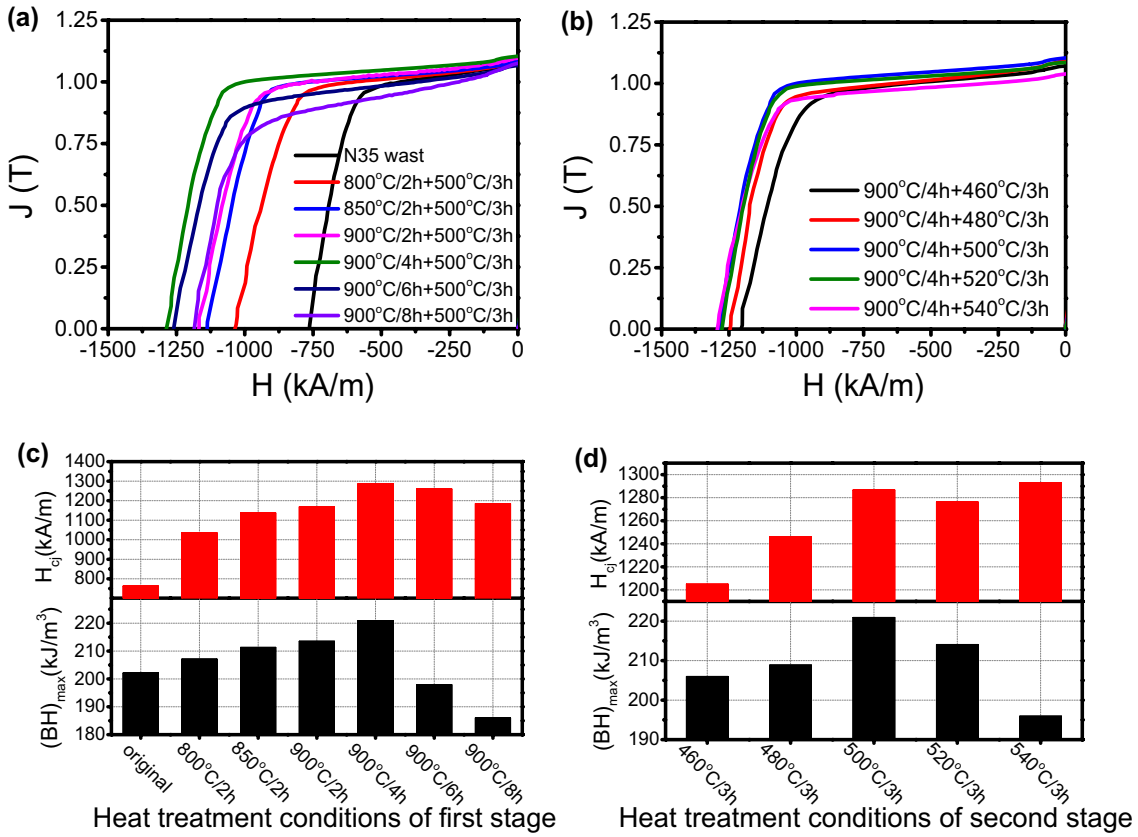

Fig. 2 Magnetic properties of the diffused magnets

at 900 °C/4 h + 500 °C/3 h. As shown in Table 2, the J_r, H_{cj} and $(BH)_{max}$ increased from 1.08 T, 763 kA/m and 202 kJ/m^3 to 1.10 T, 1287 kA/m and 221 kJ/m^3, respectively, which basically meets the standard of the N30M magnet, i.e., $J_r \geq 1.08$ T, $H_{cj} \geq 1114$ kA/m, and $(BH)_{max} \geq 223$ kJ/m^3, and are close to the standard of N30H ($H_{cj} \geq 1353$ kA/m). The great enhancement of coercivity can be easily understood, since the $Tb_2Fe_{14}B$ phase formed after diffusion has a large anisotropic field. The results also indicate that a proper diffusion heat treatment can efficiently enhance H_{cj} without a decrease of J_r and $(BH)_{max}$, despite the antiferromagnetic coupling between Tb and Fe [28]. This may be attributed to the improved squareness of demagnetization curve resulting from the optimized microstructure. The deterioration of magnetic properties by excessive diffusion, referring to the 6–8 h high temperature heat treatment, was observed. This phenomenon was also reported in other literature [29, 30], which can be attributed to the enlarged grains and severe aggregation of RE-rich phase. To further optimize the heat treatment, the second stage heat treatment with different temperatures from 460 to 540 °C were also carried out. The results in Fig. 2b, d demonstrate that 500 °C is the optimal annealing temperature in this case.

Figure 3a gives the demagnetization curves at various temperatures from 300 to 450 K for the magnet diffused at 900 °C/4 h + 500 °C/3 h. The temperature coefficients of H_{cj} ($|\beta|$) and J_r ($|\alpha|$) decrease from 0.591%/K and 0.187%/K to 0.491%/K and 0.163%/K, respectively. Here, the temperature coefficients $|\beta|$ and $|\alpha|$ are defined as $\left|\frac{H_{cj}(450\text{ K})-H_{cj}(300\text{ K})}{\Delta T \cdot H_{cj}(300\text{ K})} \times 100\%\right|$ and $\left|\frac{J_r(450\text{ K})-J_r(300\text{ K})}{\Delta T \cdot J_r(300\text{ K})} \times 100\%\right|$. According to the properties, standards for sintered NdFeB magnets, the reference values of $|\beta|$ and $|\alpha|$ for N30M in the temperature range 20–100 °C are 0.65–0.80%/K and 0.090–0.124%/K, respectively. If we extrapolate/interpolate the results in Fig. 3b to this temperature range for calculation, the diffused magnet is qualified by $|\beta|$ of 0.56%/K and $|\alpha|$ of 0.124%/K. Even more, the present magnets also meet the requirements for N30H magnets, whose reference values of $|\beta|$ and $|\alpha|$ in the temperature range 20–100 °C are 0.60–0.75%/K and 0.090–0.124%/K, respectively. This enhancement of temperature stability is also attributed to the formation of the $Tb_2Fe_{14}B$ phase. Table 2 gives the magnetic property parameters of waste magnet, optimally diffused magnet and the standards for N30 series magnets. The waste magnet has been successfully upgraded to the level close to N30H.

Figure 4a shows the EPMA mappings of the magnet after diffusion at 900 °C/4 h + 500 °C/3 h. Pr and Tb elements originally in the diffusion source were diffused from

Table 2 The magnetic properties of the studied magnets and the standards for N30 series magnets

	H_{cj} (kA/m)	J_r (T)	$(BH)_{max}$ (kJ/m^3)	$\|\alpha\|$ (%/K) (20–100 °C)	$\|\beta\|$ (%/K) (20–100 °C)
Waste magnet	763	1.08	202	0.149	0.77
GBDP treated magnet (900 °C/4 h + 500 °C/3 h)	1287	1.10	221	0.124	0.56
N30	≥ 960	≥ 1.08	≥ 223	0.090–0.124	0.70–0.82
N30M	≥ 1114	≥ 1.08	≥ 223	0.090–0.124	0.65–0.80
N30H	≥ 1353	≥ 1.08	≥ 223	0.090–0.124	0.60–0.75

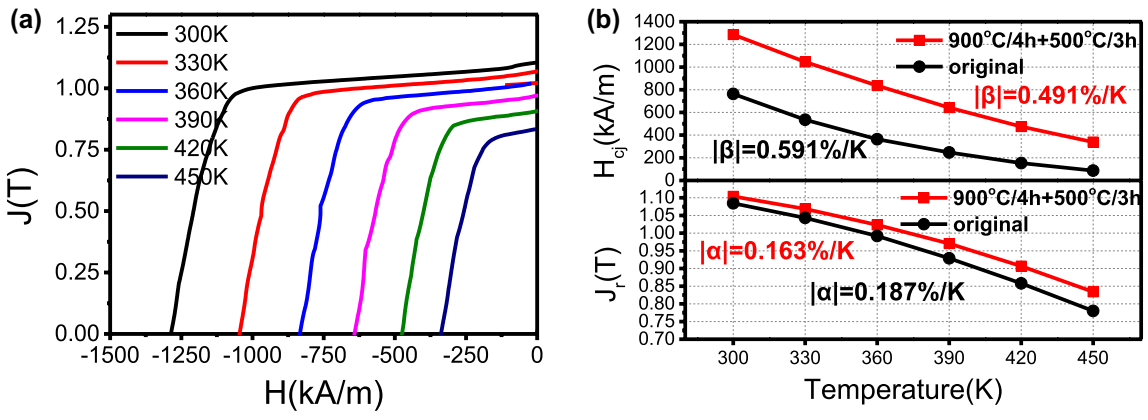

Fig. 3 **a** Demagnetization curves of the magnet after diffusion at 900 °C/4 h + 500 °C/3 h and **b** temperature stability of the magnets before and after diffusion at 900 °C/4 h + 500 °C/3 h

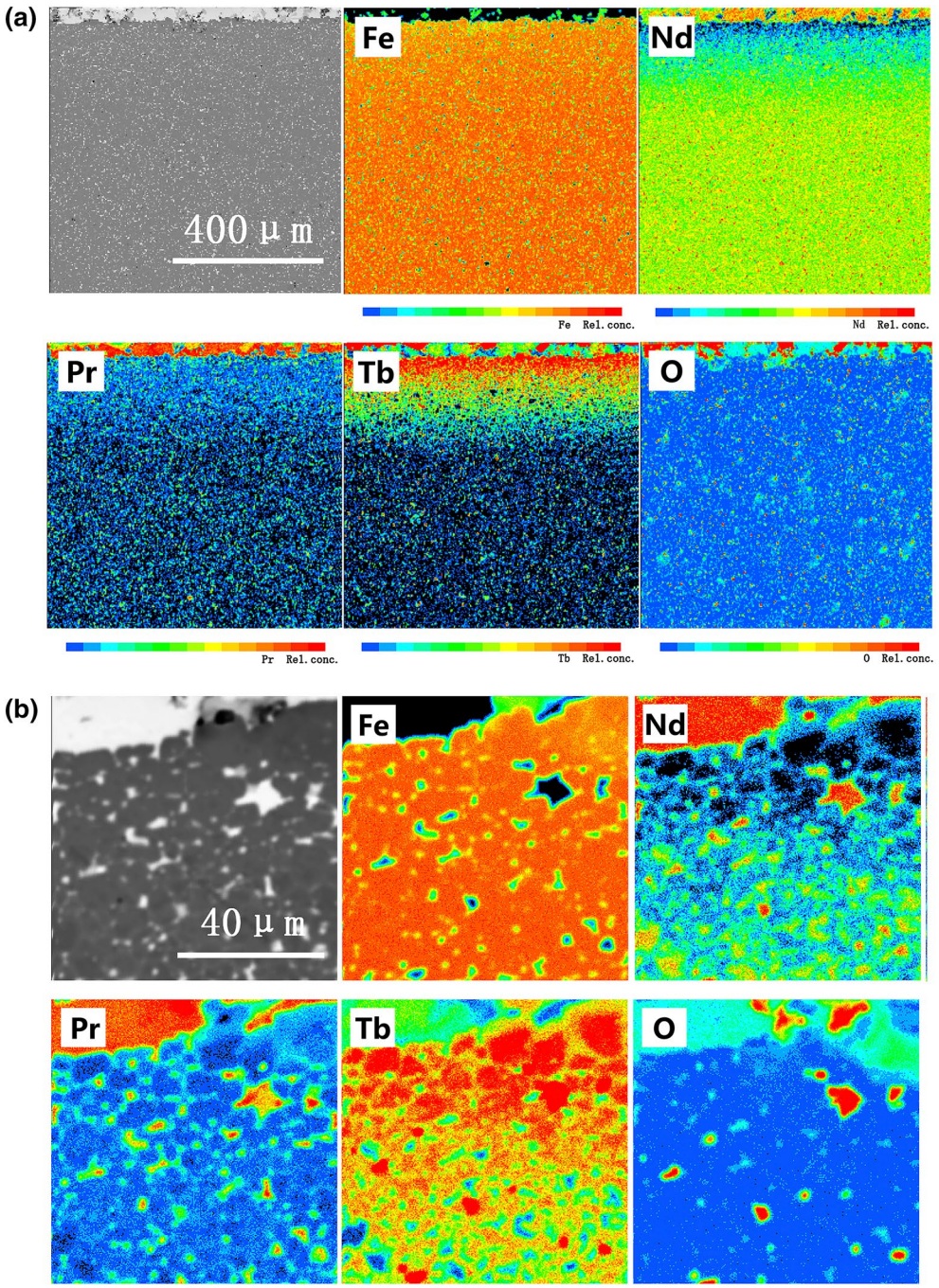

Fig. 4 EPMA images of magnet after diffusion at 900 °C/4 h + 500 °C/3 h

the surface into the magnet. It is found that the diffusion depth of Pr element is deep, whereas the Tb element is mainly concentrated within 300 μm from the surface. Also, the Nd element has a lower concentration at the surface of the magnet. It indicates that Nd was substituted by Tb and Pr, and diffused to the surface of the magnet in the opposite direction, leading to the enhancement of H_{cj} and temperature stability.

Figure 4b shows the surface region of the diffused magnets. It is widely known that, in Tb- or Dy-diffused NdFeB magnets, the typical shell/core structure of (Tb/Dy,Nd)$_2$Fe$_{14}$B grains consists of Nd$_2$Fe$_{14}$B core and Tb/Dy-rich (Tb/Dy)$_2$Fe$_{14}$B shell. But in this case, at the outermost layer of the magnet, the (Tb,LRE)$_2$Fe$_{14}$B grains are surrounded by shells with lower concentration of Tb, the so-called "anti-shell/core" structure [31]. This "anti-shell/

core" structure results from the different speeds of element in grain boundary diffusion and intergranular diffusion. At the first stage of the diffusion process, the concentration of Tb at the grain boundaries is higher than that at inner grains, leading to the inward diffusion of Tb atoms. At the second stage, such as the consumption of diffusion source and the faster speed of grain boundary diffusion, the concentration of Tb at grain boundaries is lower than that at the inner grains, which results in the outward diffusion of Tb. Li et al. [31] reported that the anti-shell/core structure has a negative effect on the coercivity of diffused magnets, based on the fact that the coercivity increased after removing the layer with the "anti-shell/core" structure [31]. In fact, the outer layer of diffusion-treated magnet tends to have more defects, such as disorientation and oxidation. It is hard to conclude whether the shell/core structure leads to a reduction of coercicity. However, one thing for sure is that this structure cannot achieve efficient use of Tb elements compared to the typical shell/core structure.

Unlike the surface region of the diffused magnet, the magnet at depth of 100 μm below the surface exhibits different microstructure and its EPMA images are shown in Fig. 5. At this depth, the magnet has clear shell/core structure. The grains consist of the cores with higher concentrations of Nd, Ce and Gd and shells with higher concentrations of Tb and Pr, which are also confirmed by the line scanning results in Fig. 7. This structure has been widely discussed and is believed to effectively improve the coercivity without a significant remanence reduction.

Since the EPMA mapping gives the concentration information of each element at the same position, we can get the composition information of each pixel in the EPMA images. Based on this idea, a statistic content variations of REEs in the main phase with depth are shown in Fig. 6, which can help us to qualitatively analyze the different diffusion behavior of each REE. The curves of Tb and Pr, which came from the diffusion source, show significant difference. The content of Tb in the main phase decreases obviously with the depth, and the content of Pr does not show significant variation. This result demonstrates that the substitution effect of the Tb element is much stronger than that of the Pr element. In terms of the Nd, Ce and Gd, their content presents an increased trend with depth, which indicates that they are replaced by the Tb and Pr. In addition, judging from the

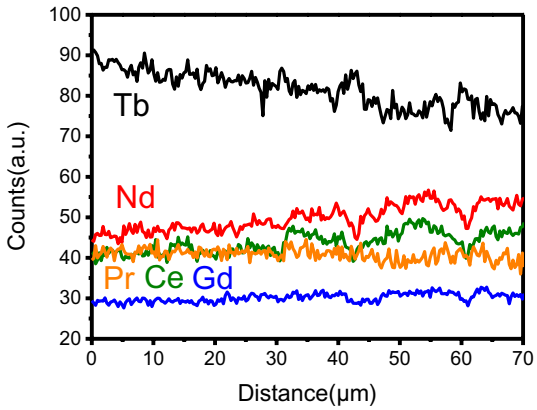

Fig. 6 Content variation of each element in the main phase with depth as calculated from Fig. 6

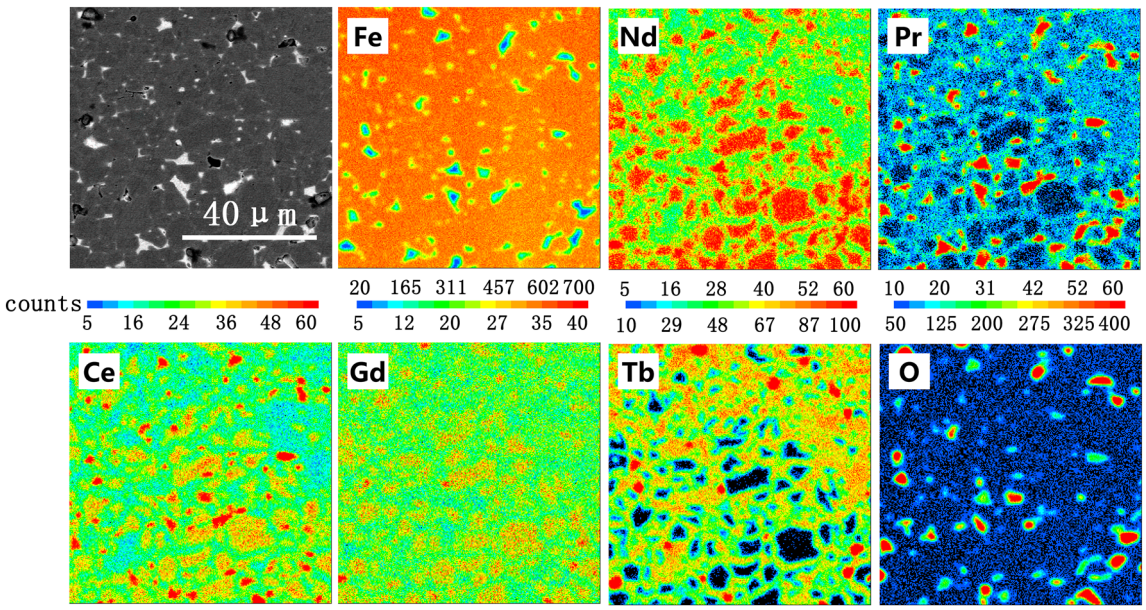

Fig. 5 EPMA images of the magnet at a distance of 100 μm from the surface after diffusion at 900 °C/4 h + 500 °C/3 h

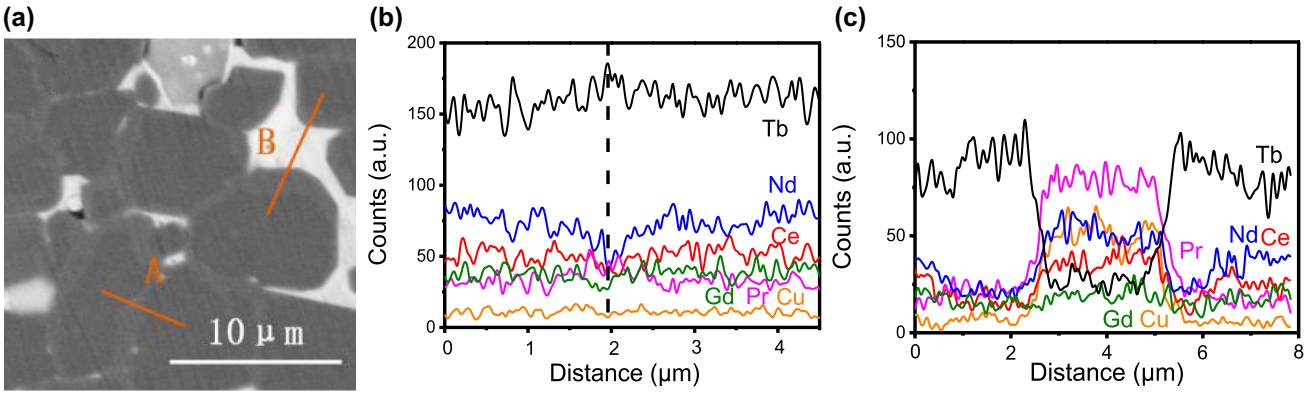

Fig. 7 **a** SEM images of the magnet at a distance of 100 μm from the surface after diffusion at 900 °C/4 h + 500 °C/3 h; concentration profiles of line scanning at **b** A and **c** B in **a**

slope of the curves, the capacity of being replaced by Nd is greater than Ce, which is greater than Gd.

The results in Fig. 6 indicate the different main phase-forming abilities for each REE. This different abilities can be further understood by analyzing the distribution preference of REEs in Fig. 7c. Unlike other REEs, Tb element prefers substituting Nd in the $Nd_2Fe_{14}B$-type main phase rather than entering into the RE-rich phase. On the contrary, other REEs, Pr, Nd, Ce and Gd, prefer forming RE-rich phase. By comparing the intensity of the element signals in the main phase and RE-rich phase, we can qualitatively rank the distribution preference of these four REEs. The tendency of distribution in the RE-rich phase from strong to weak are: Pr, Nd, Ce and Gd, which is consistent with the analysis in Fig. 6.

4 Conclusions

$Pr_{40}Tb_{30}Cu_{30}$ alloy was employed as the diffusion source to restore and enhance the coercivity of waste N30 sintered magnets containing mixed Nd and LRE elements. The relationship between microstructure evolution and coercivity enhancement was investigated. By optimized diffusion treatment, the unqualified N30 magnets was upgraded to N30M, close to N30H, and the coercivity was increased from 763 kA/m to 1287 kA/m. A two-step diffusion heat treatment generated the shell/core structure via the substitution of Nd, Ce and Gd atoms by Tb and Pr atoms, which is concluded to be the main reason for coercivity enhancement. Five REEs involved in this work show significantly different behaviors during diffusion. The Tb element prefers entering the main phase rather than staying in the RE-rich phase, while the Pr element prefers distributing in the RE-rich phase with a larger diffusion depth. In terms of the originally contained REEs, Nd, Ce and Gd, the tendency of being replaced from strong to weak is: Nd, Ce and Gd. This work demonstrates that GBDP is an effective approach for restoring and upgrading the properties of waste NdFeB magnet, providing a novel route for NdFeB waste recycling. The results of the preference of REEs distribution and substitution are believed to give a reference for the REE utilization in GBDP and other multi-REE system research.

Acknowledgements This work was partly supported by the National Natural Science Foundation of China (Grant no. 51774146) and the Guangdong Key Laboratory of Rare Earth Development and Applications (Grant no. XTKY-201801).

References

1. O. Gutfleisch, M.A. Willard, E. Bruck, C.H. Chen, S.G. Sankar, J.P. Liu, Adv. Mater. **23**, 821 (2011)
2. S. Sugimoto, J. Phys. D: Appl. Phys. **44**, 064001 (2011)
3. M. Zakotnik, C.O. Tudor, Waste Manag. **44**, 48 (2015)
4. A. Golev, M. Scott, P.D. Erskine, S.H. Ali, G.R. Ballantyne, Resour. Pol. **41**, 52 (2014)
5. Kataoka Y, Ono T, Tsubota M, Kitagawa J, AIP Adv. **5**, 117212 (2015)
6. S. Shirayama, T.H. Okabe, Metall. Mater. Trans. B **49**, 1067 (2018)
7. Y. Chen, H. Wang, Y. Pei, J. Ren, J. Wang, ACS Sustain. Chem. Eng. **3**, 3167 (2015)
8. V. Innocenzi, F. Vegliò, J. Power Sour. **211**, 184 (2012)
9. M. Itoh, K. Miura, K-i Machida, J. Alloys Compd. **477**, 484 (2009)
10. T. Uda, Mater. Trans. **43**, 55 (2002)
11. M. Zakotnik, I.R. Harris, A.J. Williams, J. Alloys Compd. **450**, 525 (2008)
12. R.S. Sheridan, R. Sillitoe, M. Zakotnik, I.R. Harris, A.J. Williams, J. Magn. Magn. Mater. **324**, 63 (2012)
13. Y. Zhang, M. Liu, S. Sun, X. Yin, Y. Yin, J. Guo, W. Liu, D. Zhang, M. Yue, J. Magn. Magn. Mater. **475**, 465 (2019)
14. H. Sepehri-Amin, T. Ohkubo, M. Zakotnik, D. Prosperi, P. Afiuny, C.O. Tudor, K. Hono, J. Alloys Compd. **694**, 175 (2017)
15. M. Itoh, M. Masuda, S. Suzuki, K-i Machida, J. Alloys Compd. **374**, 393 (2004)
16. X. Li, M. Yue, M. Zakotnik, W. Liu, D. Zhang, T. Zuo, J. Rare Earths **33**, 736 (2015)

17. M. Itoh, K. Nishiyama, F. Shogano, T. Murota, K. Yamamoto, M. Sasada, K-i Machida, J. Alloys Compd. **451**, 507 (2008)
18. H. Nakamura, K. Hirota, M. Shimao, T. Minowa, M. Honshima, IEEE Trans. Magn. **41**, 3844 (2005)
19. J. Song, S. Guo, G. Ding, K. Chen, R. Chen, D. Lee, A. Yan, J. Magn. Magn. Mater. **469**, 613 (2019)
20. K.C. Lu, X.Q. Bao, G.X. Chen, X. Mu, X.J. Zhang, X.K. Lv, Y. Ding, X.X. Gao, J. Magn. Magn. Mater. **477**, 237 (2019)
21. J. Li, L. Liu, H. Sepehri-Amin, X. Tang, T. Ohkubo, N. Sakuma, T. Shoji, A. Kato, T. Schrefl, K. Hono, Acta Mater. **161**, 171 (2018)
22. J. Di, G. Ding, X. Tang, X. Yang, S. Guo, R. Chen, A. Yan, Scripta Mater. **155**, 50 (2018)
23. J.R. Xiao, Z.W. Liu, H.S. Lou, H.X. Zhan, Acta Phys. Sin. **67**, 9 (2018)
24. S. Hirosawa, Y. Matsuura, H. Yamamoto, S. Fujimura, M. Sagawa, H. Yamauchi, J. Appl. Phys. **59**, 873 (1986)
25. Y. Zhang, T. Ma, J. Jin, J. Li, C. Wu, B. Shen, M. Yan, Acta Mater. **128**, 22 (2017)
26. X. Tang, H. Sepehri-Amin, T. Ohkubo, M. Yano, M. Ito, A. Kato, N. Sakuma, T. Shoji, T. Schrefl, K. Hono, Acta Mater. **144**, 884 (2018)
27. T. Ma, M. Yan, K. Wu, B. Wu, X. Liu, X. Wang, Z. Qian, C. Wu, W. Xia, Acta Mater. **142**, 18 (2018)
28. J.F. Herbst, Rev. Mod. Phys. **63**, 819 (1991)
29. H. Zeng, Z. Liu, W. Li, J. Zhang, L. Zhao, X. Zhong, H. Yu, B. Guo, J. Magn. Magn. Mater. **471**, 97 (2019)
30. S. Kim, D.-S. Ko, H.-S. Lee, D. Kim, J.W. Roh, W. Lee, J. Alloys Compd. **780**, 574 (2019)
31. W. Li, Q. Zhang, Q. Zhu, S. Xiao, C. Xu, L. Yang, B. Zheng, S. Mao, Z. Song, Scripta Mater. **163**, 40 (2019)